Warm non-equilibrium gas phase chemistry as a possible origin of high HDO/H2O ratios in hot and dense gases

Thi, W. -F.; Woitke, P.; Kamp, I.

Published in:
Monthly Notices of the Royal Astronomical Society

DOI:
10.1111/j.1365-2966.2009.16162.x

Publication date:
2010

Monthly Notices
of the
ROYAL ASTRONOMICAL SOCIETY

Mon. Not. R. Astron. Soc. **407,** 232–246 (2010) doi:10.1111/j.1365-2966.2009.16162.x

Warm non-equilibrium gas phase chemistry as a possible origin of high HDO/H_2O ratios in hot and dense gases: application to inner protoplanetary discs

W.-F. Thi,[1⋆] P. Woitke[2] and I. Kamp[3]

[1] *SUPA,† Institute for Astronomy, University of Edinburgh, Royal Observatory, Blackford Hill, Edinburgh EH9 3HJ*
[2] *UK Astronomy Technology Centre, Royal Observatory, Edinburgh, Blackford Hill, Edinburgh EH9 3HJ*
[3] *Kapteyn Astronomical Institute, Postbus 800, 9700 AV Groningen, the Netherlands*

Accepted 2009 December 3. Received 2009 December 3; in original form 2009 February 12

ABSTRACT

The origin of Earth oceans is controversial. Earth could have acquired its water either from hydrated silicates (wet Earth scenario) or from comets (dry Earth scenario). [HDO]/[H_2O] ratios are used to discriminate between the scenarios. High [HDO]/[H_2O] ratios are found in Earth oceans. These high ratios are often attributed to the release of deuterium enriched cometary water ice, which was formed at low gas and dust temperatures. Observations do not show high [HDO]/[H_2O] in interstellar ices. We investigate the possible formation of high [HDO]/[H_2O] ratios in dense ($n_H > 10^6$ cm^{-3}) and warm gas ($T = 100$–1000 K) by gas-phase photochemistry in the absence of grain surface chemistry. We derive analytical solutions, taking into account the major neutral–neutral reactions for gases at $T > 100$ K. The chemical network is dominated by photodissociation and neutral–neutral reactions. Despite the high gas temperature, deuterium fractionation occurs because of the difference in activation energy between deuteration enrichment and the back reactions. The analytical solutions were confirmed by the time-dependent chemical results in a 10^{-3} $M_\odot$ disc around a typical T Tauri star using the photochemical code ProDiMo. The ProDiMo code includes frequency-dependent 2D dust-continuum radiative transfer, detailed non-local thermodynamic equilibrium gas heating and cooling and hydrostatic calculation of the disc structure. Both analytical and time-dependent models predict high [HDO]/[H_2O] ratios in the terrestrial planet-forming region (<3 au) of circumstellar discs. Therefore, the [HDO]/[H_2O] ratio may not be an unique criterion to discriminate between the different origins of water on the Earth.

Key words: astrochemistry.

1 INTRODUCTION

The water deuteration abundance ratio [HDO]/[H_2O] is often used to determine the temperature at which water was synthesized. Current submillimetre observations already provide measurements of [HDO]/[H_2O] for many astronomical objects including comets, hot cores and protoplanetary discs. In particular, a high [HDO]/[H_2O] has been observed toward the protoplanetary disc DM Tau (Ceccarelli et al. 2005), although the HDO detection remains controversial (Guilloteau et al. 2006). The *Herschel Space Telescope* will be capable to detect cool and warm water in discs while the Atacama Large Millimeter Array will spatially resolve HDO emission.

The water deuteration abundance ratio [HDO]/[H_2O] in hot cores around massive young stellar objects is $\sim 3 \times 10^{-4}$ (Gensheimer, Mauersberger & Wilson 1996), around a factor of $\sim$10 enhancement compared to the cosmic [D]/[H] value set at the big bang ($\sim 1.5 \times 10^{-5}$; Linsky 2003). The enrichment suggests that the chemistry occurs in a low-density, cold medium ($T < 100$ K), where HDO synthesis begins with the deuteration of the molecular ion H_3^+ into H_2D^+ (e.g. Roberts & Millar 2000). Further gas-phase reactions lead to a high [HDO]/[H_2O]. However, at temperatures greater than 100 K, which is the typical gas temperature of hot cores, the initial deuteration reaction is inefficient and the [HDO]/[H_2O] is close to the cosmic value. Therefore, current chemical models need to invoke the evaporation of deuterium enriched water ice when the temperature reaches 100 K to explain the deuterium enrichment in water. The observed (HDO/H_2O) ice ratio is however

⋆E-mail: thiw@ujf-grenoble.fr
†Scottish Universities Physics Alliances.

too low (Dartois et al. 2003; Parise et al. 2003). A second difficulty arises from the high observed water ice abundance of 10^{-5}–10^{-4}, which is two orders of magnitude larger than the gas phase abundance of water in the hot core around IRAS 16293−2422 (Parise et al. 2005).

After decades of research, the origin of water on the Earth remains a major subject of debate (e.g. Nuth 2008 for a review). Two major models exist. In the first model, the Earth accretes dry: the building blocks of the Earth are made of dry rocks, composed only of silicates and carbonaceous materials. Most of the water is brought afterward by comets during the phase of heavy bombardment. This model is supported by the similarity between the Earth Mean Ocean Water (SMOW $\simeq 1.49 \times 10^{-4}$) [HDO]/[$H_2O$] and the cometary value, although the later value seems too high. Another support to the 'dry' model is the low [HDO]/[H_2O] predicted at temperature $T > 100$ K by thermochemical equilibrium models. In the second model, most of the water on the Earth comes from the release of water vapour trapped inside the water-entrapped planetesimals like carbonaceous chondrites upon impact or during volcanism. Water-rich planetesimals located at 2–3 au are perturbed by the giant planets and collide with the young Earth (Morbidelli et al. 2000; Raymond, Quinn & Lunine 2004, 2005; Gomes et al. 2005). Those planetesimals contain water in the form of hydrated silicates. The average D/H in carbonaceous chrondrite is similar to the value in the Earth ocean (Robert, Gautier & Dubrulle 2000), although the composition of carbonaceous chrondrite does not match the composition of the Earth's crust (Righter, Drake & Scott 2006). The Earth is said to have accreted 'wet' (Drake 2005). Hydrous material does not necessarily needed to be brought from the asteroid belt area (2–3 au). Recent study on adsorption of water molecules on to fractal dust grains shows that hydrous material could have been present in the vicinity of 1 au (Stimpfl et al. 2006). In this scenario, water in the gaseous solar nebula sticks on to the silicate surface of fractal grains, which coagulate and grow into the Earth. The adsorbed water would reflect the deuterium enrichment of the gas-phase water at 1 au. The major difference between the two 'wet' scenarios is that water was present in the early Earth in the latter scenario. Geochemical findings suggest that hydrosphere and continental crust were already present in the first ∼600 Myr of the Earth history (Hopkins, Harrison & Manning 2008). The presence of water and also of organic matter at the formation of the Earth has profound astrobiology implications for the origin of life.

One major weakness of the 'wet' scenario is that the deuterium enrichment predicted by equilibrium chemistry is too low at temperatures greater than 100 K. However, there are chemical routes to obtain high [HDO]/[H_2O] ratios at temperatures greater than 100 K in non-equilibrium chemistry. Photodissociation of H_2O and HDO followed by reformation at the surface of protoplanetary discs and turbulent mixing can also change the [HDO]/[H_2O] (Yung et al. 1988). Vertical turbulent mixing was invoked by Lyons & Young (2005) to explain the oxygen anomalies in the early solar nebula. Alternatively, Genda & Ikoma (2008) propose that the [HDO]/[H_2O] ratio on the Earth changed during the evolution of the Earth from its formation. Willacy & Woods (2009) studied the deuterium chemistry of the inner disc around a T Tauri star and found relatively high HDO abundance in the warm molecular layer.

Four direct physical processes lead to isotopic fractionation in the gas phase. First, heavier isotopologues diffuse slower than the lighter main isotopologue. The diffusion results in zones of varying [HDO]/[H_2O] ratios. This process is negligible in turbulent media when the mixing time-scale is much lower than the diffusion time-scales. Secondly, due to their larger reduced mass, isotopologues usually have a lower zero-point energy. The vibrational energy levels are located lower, which increases the density sum of energy and hence reduces the vapour pressure. Hence, the water ice/gas ratios in the interstellar medium (ISM) are not at equilibrium. Thirdly, heavier isotopologues are chemically more stable because the binding energy between O and D is stronger than between O and H in the water molecule. Fractionation reactions dominate at low temperature because the inverse reactions have a minimum energy barrier equal to the difference in binding energy. Finally, isotopologues differ in their photodissociation cross-section due to changes in the selection rules. A combination of the last two processes together with chemical diffusion and turbulent mixing probably determines the deuterium fractionation in the inner region of protoplanetary discs, where terrestrial planets form.

Interstellar chemical models often neglect or include only few neutral–neutral reactions because their rates are small at temperatures below ∼100 K, but they become competitively fast with the ion–neutral reactions at a few hundred degrees. For example, in dense and warm gases, the central species is the hydroxyl radical OH, which can react with H_2 to form H_2O (Thi & Bik 2005).

In this paper, we explore neutral–neutral and photochemical reactions relevant to the formation and destruction of H_2, HD, OH, OH, H_2O and HDO at gas temperature between 100 and 1000 K. We first focus on steady-state abundances and perform an analytical analysis. Analytical analysis makes it possible to determine the main formation and destruction paths. After establishing the possible reaction paths, we use the photochemical code ProDiMo to compute a time-dependent chemical structure for a typical T Tauri disc to check the validity of our assumptions in the analytical analysis. In the rest of the paper, the chemical reaction rates are given in Tables 1–5. In particular, the most important reactions are summarized in Table 1.

2 STEADY-STATE ANALYTICAL SOLUTION

2.1 Formation and destruction of H_2O and HDO

We consider a gas mixture at a single temperature, density, irradiated by ultraviolet (UV) photons. In thermochemical equilibrium the deuterium exchange equilibrium reaction between water and molecular hydrogen (the most abundant reservoir of deuterium) is (e.g. Robert et al. 2000)

$$\mathrm{HD} + \mathrm{H_2O} \leftrightarrow \mathrm{HDO} + \mathrm{H_2}. \quad (1)$$

Table 1. Principal reactions.

	Reaction	A ($cm^3\ s^{-1}$)	B	E_a (K)	Reference
k_1	$O + H_2 \rightarrow OH + H$	3.14×10^{-13}	2.7	3150	Woodall et al. (2007)
k_5	$OH + H_2 \rightarrow H_2O + H$	2.05×10^{-12}	1.52	1660	Woodall et al. (2007)
k_{10}	$H_2 + D \rightarrow HD + H$	7.50×10^{-11}	–	3820	Zhang & Miller (1989)
k_{11}	$HD + H \rightarrow H_2 + D$	7.50×10^{-11}	–	4240	Zhang & Miller (1989)
k_{12}	$O + HD \rightarrow OD + H$	1.57×10^{-12}	1.7	4639	Joseph, Truhlar & Garret (1988)
k_{16}	$OH + D \rightarrow OD + H$	9.07×10^{-11}	−0.63	–	Yung et al. (1988)
k_{20}	$OH + HD \rightarrow HDO + H$	0.60×10^{-13}	1.9	1258	Talukdar et al. (1996)
k_{22}	$OD + H_2 \rightarrow HDO + H$	1.55×10^{-12}	1.6	1663	Talukdar et al. (1996)
	Reaction	q	γ (s^{-1})		Reference
J_2	$HD + h\nu \rightarrow H + D$	2.6×10^{-11}	2.5	–	Le Petit et al. (2002)
J_4	$OH + h\nu \rightarrow O + H$	3.5×10^{-10}	1.7	–	van Dishoeck (1988)

The equilibrium constant (K) of this reaction for gas at temperature between 273 and 1000 K is (Richet, Bottinga & Janoy 1977)

$$K = \frac{P_{\rm HDO} P_{\rm H_2}}{P_{\rm HD} P_{\rm H_2O}} \simeq \frac{0.22 \times 10^6}{T^2} + 1. \quad (2)$$

The pressure dependence of K is negligible. At equilibrium, the deuterium enrichment decreases quadratically with temperature. A gas mixture is in thermochemical equilibrium when each chemical reaction is exactly balanced by its reverse reaction. Dissociations upon absorption of UV photons are not taken into account.

A gas is in chemical steady state (also called stationary state) if the various abundances do not vary with time but the formation and destruction reactions for a given species are not necessarily the same. An analytical solution to the chemical network for the synthesis of H_2O and HDO can be obtained by identifying the main formation and destruction chemical reactions. At high temperature ($T > 100$ K) and density, it is well established that water is primarily formed via the reactions between the hydroxyl radical OH and molecular hydrogen H_2 (e.g. Thi & Bik 2005; Glassgold, Meijerink & Najita 2009). High-temperature gases are needed to overcome the large energy barrier of the reaction (reaction 5 with rate k_5, $E_a = 1660$ K). The main destruction mechanism is likely photodissociation in low A_V regions. Other water destruction mechanisms are reactions with atomic hydrogen and with ionized helium in shielded regions. We assume in this study that the dust temperature T_d has equilibrated with the gas temperature. At $T_d > 100$ K, most water molecules remain in the gas phase. The rate of water formation is thus

$$\frac{{\rm d}[H_2O]}{{\rm d}t} = (k_5[H_2] + k_{18}[HD] + k_7[OH])[OH] - (J_6 + k_8[H] + k_{19}[D] + k_{41}[He^+] + k_{\rm cp,3})[H_2O], \quad (3)$$

where k_5, k_{18} and k_7 are the rates of formation of water via the reactions OH + H_2, OH + HD and OH + OH, respectively, J_6 is the photodissociation rate, k_8 is the water destruction rate by H, $k_{\rm cp,3}$ is the cosmic ray induced photodissociation of water and k_{41} is the rate of destruction by He^+. At steady state (${\rm d}[H_2O]/{\rm d}t = 0$), we obtain the ratio

$$\frac{[H_2O]}{[OH]} \simeq \frac{k_5[H_2]}{J_6 + k_8[H] + k_{41}[He^+] + k_{\rm cp,3}}, \quad (4)$$

which will be used later in this paper. We have neglected the formation of water via reaction of OH with HD and OH, and destruction of water via atomic deuterium because the rates are of the orders of magnitude smaller than the rates of other paths. Deuterated water can be formed via the reaction of HD with OH as well as via OD + H_2 (Bergin, Neufeld & Melnick 1998). Destruction occurs via photodissociation, reaction with atomic hydrogen and ionized helium:

$$\frac{{\rm d}[HDO]}{{\rm d}t} = k_{22}[OD][H_2] + k_{20}[OH][HD] - (J_{7a} + J_{7b} + (k_{21} + k_{23})[H] + (k_{42} + k_{43})[He^+] + k_{\rm cp,4} + k_{\rm cp,5})[HDO]. \quad (5)$$

The photodissociation of HDO can either lead to OH + D (J_{7a}) or to OD + H (J_{7b}). The sum of the two photo rates is the total HDO photodissociation rate and is similar to the H_2O photodissociation rate J_6. The photodissociation of HDO favours cleavage of the O–H bond over O–D bond with a 3 to 1 ratio (Shafer, Satyapal & Bersohn 1989; Vander Wal, Scott & Crim 1990; Vander Wal et al. 1991), i.e. $J_{7b} \simeq 3J_{7a}$ because the binding energy between O and D is stronger than that of between O and H in water. In steady state, the balance between formation and destruction leads to the ratio

$$X_D = \frac{[HDO]}{[H_2O]} = \frac{(k_{22}[OD][H_2] + k_{20}[OH][HD])/(J_{7a} + J_{7b} + (k_{21} + k_{23})[H] + (k_{42} + k_{43})[He^+] + k_{\rm cp,4} + k_{\rm cp,5})}{k_5[OH][H_2]/(J_6 + k_8[H] + k_{41}[He^+] + k_{\rm cp,3})}, \quad (6)$$

$$X_D = \frac{[HDO]}{[H_2O]} = \left(\frac{D_{\rm H_2O}}{D_{\rm HDO}}\right)\left(\frac{k_{22}([OD]/[OH])[H_2] + k_{20}[HD]}{k_5[H_2]}\right), \quad (7)$$

where we define

$$D_{\rm H_2O} = J_6 + k_8[H] + k_{41}[He^+] + k_{\rm cp,3} \quad (8)$$

and

$$D_{\rm HDO} = J_{7a} + J_{7b} + (k_{21} + k_{23})[{\rm H}] + (k_{42} + k_{43})[{\rm He}^+] + k_{\rm cp,4} + k_{\rm cp,5} \tag{9}$$

to be the total destruction rates of H_2O and HDO. The total UV photodissociation rates of H_2O and HDO are similar (Zhang & Imre 1988): $J_6 \simeq J_{7a} + J_{7b}$. We further assume that rates with the deuterated species are similar to that of the main isotopologues: $k_8 = k_{21} + k_{23}, k_{41} \simeq k_{42} + k_{43}$ and $k_{\rm cp,4} + k_{\rm cp,5} = k_{\rm cp,3}$. If we can make the assumption that the total destruction rates of H_2O and HDO are similar, i.e. $D_{\rm H_2O} \simeq D_{\rm HDO}$, then the value of [HDO]/[H_2O] does not depend on the actual destruction mechanisms for H_2O and HDO. The water fractionation f(HDO) is defined as

$$f({\rm HDO}) = \frac{[{\rm HDO}]/[{\rm H_2O}]}{[{\rm HD}]/[{\rm H_2}]} = \left(\frac{D_{\rm H_2O}}{D_{\rm HDO}}\right)\left(\frac{k_{22}}{k_5}\frac{[{\rm OD}]/[{\rm OH}]}{[{\rm HD}]/[{\rm H_2}]} + \frac{k_{20}}{k_5}\right) = \left(\frac{D_{\rm H_2O}}{D_{\rm HDO}}\right)\left(\frac{k_{22}}{k_5} f({\rm OD}) + \frac{k_{20}}{k_5}\right) \simeq \frac{k_{22}}{k_5} f({\rm OD}) + \frac{k_{20}}{k_5}. \tag{10}$$

The ratio k_{20}/k_5 is the ratio between the reaction of OH with HD to form HDO compared to the reaction of OH with H_2 to form water. From the values in Table 1, the k_{20}/k_5 ratio is lower than 1 for gas temperature greater than 120 K. This term does not enhance the water deuteration fractionation. We can write analytically the ratio between rate k_{22} and rate k_5:

$$\frac{k_{22}}{k_5} = \frac{1.55 \times 10^{-12}(T/300)^{1.6}\ {\rm e}^{-1663/T}}{2.05 \times 10^{-12}(T/300)^{1.52}\ {\rm e}^{-1660/T}} = 0.756098(T/300)^{0.08}\ {\rm e}^{-3/T}. \tag{11}$$

The ratio is weakly temperature dependant. Since $k_{22}/k_5 = 0.7$–1 between 100 and 1000 K, water and hydroxyl radical deuterium fraction are similar at gas temperature greater than ∼200 K: f(HDO) ≃ f(OD). Therefore, water would be deuterium fractionated if OH is [i.e. f(OD) > 1].

2.2 Formation and destruction of OH and OD

The water deuteration fraction f(HDO) is intimately linked to that OH f(OD). The rate limiting reaction for the formation of water is the formation of hydroxyl radical OH: O + H_2 → OH + H with rate k_1. This reaction has a large energy barrier (E_a = 3163 K). The chemistry of OD (and OH) is described in details by Croswell & Dalgarno (1985) for reactions without barrier. The production of OD mostly occurs through the rapid exchange reaction,

$$\rm D + OH \rightarrow OD + H, \tag{12}$$

once OH is present in the gas (reaction 16 with rate from Yung et al. 1988). The forward reaction has no activation barrier but the reverse reaction (reaction 13) has a barrier of 810 K because OD is more stable than OH. Thus at $T < 1000$ K, OD is favoured. The role of OD for gas between 100 and 1000 K is similar to that of H_2D^+ for gas at $T < 100$ K for the deuterium enrichment. OD can also formed by the reaction

$$\rm HD + O \rightarrow OD + H. \tag{13}$$

OD is destroyed by reaction with carbon ion

$$\rm C^+ + OD \rightarrow CO + D^+, \tag{14}$$

$$\rm C^+ + OD \rightarrow CO^+ + D, \tag{15}$$

and by photodissociation (with rate J_5)

$$\rm OD + h\nu \rightarrow O + D. \tag{16}$$

The steady-state abundance of OH and OD taking into account the most important formation and destruction reactions are

$$[{\rm OH}] = \frac{k_1[{\rm O}][{\rm H_2}] + (J_6 + k_8[{\rm H}] + k_{41}[{\rm He}^+] + k_{\rm cp,3})[{\rm H_2O}] + k_{14}[{\rm O}][{\rm HD}] + k_{22}[{\rm OD}][{\rm H_2}] + k_{30}[{\rm CO}][{\rm H}] + (J_{7a} + k_{\rm cp,5})[{\rm HDO}]}{(k_{15} + k_{16})[{\rm D}] + k_4[{\rm H}] + k_5[{\rm H_2}] + k_{44}[{\rm He}^+] + k_6[{\rm O}] + k_{26}[{\rm OD}] + k_{28}[{\rm CO}] + k_{29}[{\rm C}] + k_{39}[{\rm C}^+] + J_4 + k_{\rm cp,1}}, \tag{17}$$

$$[{\rm OH}] \simeq \frac{k_1[{\rm O}][{\rm H_2}]}{k_4[{\rm H}] + k_5[{\rm H_2}] + k_{28}[{\rm CO}] + J_4 + k_{\rm cp,1} + k_{29}[{\rm C}] + k_{39}[{\rm C}^+]}. \tag{18}$$

After some algebra, we obtain the ratio

$$\frac{[{\rm OH}]}{[{\rm O}]} \simeq \frac{k_1[{\rm H_2}]}{J_4 + k_4[{\rm H}] + k_{28}[{\rm CO}] + k_{\rm cp,1} + k_{29}[{\rm C}] + k_{39}[{\rm C}^+] + k_{44}[{\rm He}^+] + k_{\rm cp,1}}, \tag{19}$$

which would be useful later in the analysis. For the deuterated hydroxyl radical at steady state:

$$[{\rm OD}] = \frac{k_{16}[{\rm OH}][{\rm D}] + k_{12}[{\rm O}][{\rm HD}] + k_{23}[{\rm HDO}][{\rm H}] + k_{25}[{\rm O_2}][{\rm D}] + k_{27}[{\rm HDO}][{\rm O}] + k_{33}[{\rm CO}][{\rm D}] + (J_{7b} + k_{\rm cp,4})[{\rm HDO}]}{k_{17}[{\rm H}] + k_{22}[{\rm H_2}] + k_{45}[{\rm He}^+] + k_{24}[{\rm O}] + k_{26}[{\rm OH}] + k_{31}[{\rm CO}] + k_{32}[{\rm C}] + k_{40}[{\rm C}^+] + J_5 + k_{\rm cp,2}}. \tag{20}$$

The rates are listed in Tables 1–5. Neglecting the minor formation and destruction reactions (i.e. reactions with C and C^+), we simplify the ratio:

$$\frac{[{\rm OD}]}{[{\rm OH}]} \simeq \frac{D_{\rm OH}}{D_{\rm OD}}\left(\frac{k_{16}[{\rm OH}][{\rm D}] + k_{12}[{\rm O}][{\rm HD}] + (J_{7b} + k_{23}[{\rm H}] + k_{\rm cp,4})[{\rm HDO}]}{k_1[{\rm O}][{\rm H_2}] + (J_6 + k_8[{\rm H}] + k_{\rm cp,3})[{\rm H_2O}]}\right), \tag{21}$$

Table 2. Neutral–neutral and radical–neutral reactions.

	Reaction	A ($cm^3\ s^{-1}$)	B (K)	E_a (K)	Reference
R_1	$H + H + M \rightarrow H_2$	–	–	–	see text
R_2	$H + D + M \rightarrow HD$	–	–	–	see text
k_1	$O + H_2 \rightarrow OH + H$	3.14×10^{-13}	2.70	3150	UMIST
k_2	$O_2 + H \rightarrow OH + H$	2.61×10^{-10}	–	8156	UMIST
k_3	$O_2 + H_2 \rightarrow OH + OH$	3.16×10^{-10}	–	21890	UMIST
k_4	$OH + H \rightarrow O + H_2$	7.00×10^{-14}	2.80	1950	UMIST
k_5	$OH + H_2 \rightarrow H_2O + H$	2.05×10^{-12}	1.52	1660	UMIST
k_6	$OH + O \rightarrow O_2 + H$	1.77×10^{-11}	–	−178	UMIST
k_7	$OH + OH \rightarrow O + H_2O$	3.87×10^{-13}	1.69	−469	UMIST
k_8	$H_2O + H \rightarrow OH + H_2$	1.59×10^{-11}	1.20	9610	UMIST
k_9	$H_2O + O \rightarrow OH + OH$	1.85×10^{-11}	0.95	8571	UMIST
k_{10}	$H_2 + D \rightarrow HD + H$	7.50×10^{-11}	–	3820	Zhang & Millar (1989)
k_{11}	$HD + H \rightarrow H_2 + D$	7.50×10^{-11}	–	4240	Zhang & Millar (1989)
k_{12}	$O + HD \rightarrow OD + H$	1.57×10^{-12}	1.7	4639	Joseph, Truhlar & Garret (1988)
k_{13}	$OD + H \rightarrow O + HD$	–	–	–	$k_{13} = k_4$ is assumed
k_{14}	$O + HD \rightarrow OH + D$	9.01×10^{-13}	1.9	3730	Joseph, Truhlar & Garret (1988)
k_{15}	$OH + D \rightarrow O + HD$	–	–	–	$k_{15} = k_4$ is assumed
k_{16}	$OH + D \rightarrow OD + H$	9.07×10^{-11}	-0.63	–	Yung et al. (1988)
k_{17}	$OD + H \rightarrow OH + D$	1.26×10^{-10}	-0.63	717	Yung et al. (1988)
k_{18}	$OH + HD \rightarrow H_2O + D$	2.12×10^{-13}	2.7	1258	Talukdar et al. (1996)
k_{19}	$H_2O + D \rightarrow OH + HD$	–	–	–	$k_{19} = k_8$ is assumed
k_{20}	$OH + HD \rightarrow HDO + H$	0.60×10^{-13}	1.9	1258	Talukdar et al. (1996)
k_{21}	$HDO + H \rightarrow OH + HD$	–	–	–	$k_{21} = 0.5 \times k_8$ is assumed
k_{22}	$OD + H_2 \rightarrow HDO + H$	1.55×10^{-12}	1.6	1663	Talukdar et al. (1996)
k_{23}	$HDO + H \rightarrow OD + H_2$& –	–	–	$k_{23} = 0.5 \times k_8$ is assumed	
k_{24}	$OD + O \rightarrow O_2 + D$	–	–	–	$k_{24} = k_6$ is assumed
k_{25}	$O_2 + D \rightarrow OD + O$	–	–	–	$k_{25} = k_2$ is assumed
k_{26}	$OD + OH \rightarrow O + HDO$	–	–	–	$k_{26} = k_7$ is assumed
k_{27}	$HDO + O \rightarrow OD + OH$	–	–	–	$k_{27} = k_9$ is assumed
k_{28}	$OH + CO \rightarrow CO_2 + H$	1.17×10^{-13}	0.95	−74.0	UMIST
k_{29}	$OH + C \rightarrow CO + H$	1.10×10^{-10}	0.5	0.0	UMIST
k_{30}	$CO + H \rightarrow OH + C$	1.10×10^{-10}	0.5	77700.0	UMIST
k_{31}	$OD + CO \rightarrow CO_2 + D$	–	–	–	$k_{31} = k_{28}$ is assumed
k_{32}	$OD + C \rightarrow CO + D$	–	–	–	$k_{32} = k_{29}$ is assumed
k_{33}	$CO + D \rightarrow OD + C$	–	–	–	$k_{33} = k_{30}$ is assumed

Ref. UMIST: Woodall et al. (2007).

Table 3. Photodissociation and photoionization reactions.

	Reaction	q (s^{-1})	γ	Reference
J_1	$H_2 + h\nu \rightarrow H + H$	3.4×10^{-11}	2.5	Self-shielding factor, see text
J_2	$HD + h\nu \rightarrow H + D$	2.6×10^{-11}	2.5	Le Petit et al. (2002)
J_3	$CO + h\nu \rightarrow C + O$	2.0×10^{-10}	2.5	UMIST
J_4	$OH + h\nu \rightarrow O + H$	3.5×10^{-10}	1.7	van Dishoeck (1988)
J_5	$OD + h\nu \rightarrow O + D$	4.0×10^{-10}	1.7	Croswell & Dalgarno (1985)
J_6	$H_2O + h\nu \rightarrow H + OH$	5.9×10^{-10}	1.7	UMIST
J_{7a}	$HDO + h\nu \rightarrow OH + D$	–	–	$J_{7a} = 0.25\ J_6$, see text
J_{7b}	$HDO + h\nu \rightarrow OD + H$	–	–	$J_{7b} = 0.75\ J_6$, see text
J_9	$C + h\nu \rightarrow C^+ + e$			UMIST

Ref. UMIST: Woodall et al. (2007).

where

$$\frac{D_{OH}}{D_{OD}} = \frac{(k_{15} + k_{16})[D] + k_4[H] + k_5[H_2] + k_{44}[He^+] + k_6[O] + k_{26}[OD] + k_{28}[CO] + k_{29}[C] + k_{39}[C^+] + J_4 + k_{cp,1}}{k_{17}[H] + k_{22}[H_2] + k_{45}[He^+] + k_{24}[O] + k_{26}[OH] + k_{31}[CO] + k_{32}[C] + k_{40}[C^+] + J_5 + k_{cp,2}} \quad (22)$$

is the ratio between the sum of all destruction rates of OH and that of OD. The photodissociation rate of OH (rate J_4) and OD (rate J_5) are close (van Dishoeck & Dalgarno 1984; Croswell & Dalgarno 1985; van Dishoeck 1988) ($J_4 \simeq J_5$). From Table 1, reactions (5) and (22) have similar rates ($k_5 \simeq k_{22}$). Reactions (52) and (53) are ion–molecule reactions and we expect the rates to be of the same order of magnitude.

Table 4. Ion–neutral reactions.

	Reaction	k (cm^3 s^{-1})	Reference
k_{34}	$H^+ + D \rightarrow D^+ + H$	$1.0 \times 10^{-9}\, e^{-41/T}$	Watson (1976), UMIST
k_{35}	$He^+ + H_2 \rightarrow H + H^+ + He$	$1.1 \times 10^{-13}(T/300)^{-0.24}$	UMIST
k_{36}	$HD + H^+ \rightarrow D^+ + H_2$	$1.0 \times 10^{-9}\, e^{-464/T}$	UMIST
k_{37}	$H_2 + D^+ \rightarrow H^+ + HD$	2.1×10^{-9}	UMIST
k_{38}	$H + D^+ \rightarrow H^+ + D$	1.0×10^{-9}	Watson (1976), UMIST
k_{39}	$OH + C^+ \rightarrow CO^+ + H$	7.7×10^{-10}	Prasad & Huntress (1980), UMIST
k_{40}	$OD + C^+ \rightarrow CO^+ + D$	–	$k_{40} = k_{39}$ is assmued
k_{41}	$He^+ + H_2O \rightarrow OH + He + H^+$	6.0×10^{-11}	UMIST
k_{42}	$He^+ + HDO \rightarrow OD + He + H^+$	–	$k_{42} = 0.75k_{41}$ is assumed
k_{43}	$He^+ + HDO \rightarrow OH + He + D^+$	–	$k_{43} = 0.25k_{41}$ is assumed
k_{44}	$He^+ + OH \rightarrow O^+ + He + H$	1.1×10^{-9}	UMIST
k_{45}	$He^+ + OD \rightarrow O^+ + He + D$	–	$k_{45} = k_{44}$ is assmued

Ref. UMIST: Woodall et al. (2007).

Table 5. Cosmic ray induced ionization and recombination reactions ($\zeta = 5 \times 10^{-17}$ s^{-1}).

	Reaction	k (cm^3 s^{-1})	Reference
$k_{\zeta,1}$	$H + cr \rightarrow H^+ + e^-$	$0.46 \times \zeta$	UMIST
$k_{\zeta,2}$	$D + cr \rightarrow D^+ + e^-$	$0.46 \times \zeta$	UMIST
$k_{\zeta,3}$	$He + cr \rightarrow He^+ + e^-$	$0.5 \times \zeta$	UMIST
$k_{\zeta,4}$	$H_2 + cr \rightarrow H^+ + H + e^-$	$0.04 \times \zeta$	UMIST
$k_{\zeta,5}$	$HD + cr \rightarrow H^+ + D + e^-$	–	$k_{\zeta,5} = 0.5\, k_{\zeta,4}$ is assumed
$k_{\zeta,6}$	$HD + cr \rightarrow D^+ + H + e^-$	–	$k_{\zeta,6} = 0.5\, k_{\zeta,4}$ is assumed
$k_{e^-,1}$	$H^+ + e^- \rightarrow H + h\nu$	$3.5 \times 10^{-12}(T/300)^{-0.70}$	Prasad & Huntress (1980)
$k_{e^-,2}$	$D^+ + e^- \rightarrow D + h\nu$	–	$k_{e^-,2} = k_{e^-,1}$ is assumed
$k_{e^-,3}$	$He^+ + e^- \rightarrow He + h\nu$	$4.5 \times 10^{-12}(T/300)^{-0.67}$	Prasad & Huntress (1980)
$k_{cp,1}$	$OH + CRPhot \rightarrow O + H$	$1.3 \times 10^{-17}(509/(1-w))$	UMIST
$k_{cp,2}$	$OD + CRPhot \rightarrow O + D$	$1.3 \times 10^{-17}(509/(1-w))$	$k_{cp,2} = k_{cp,1}$ is assumed
$k_{cp,3}$	$H_2O + CRPhot \rightarrow OH + H$	$1.3 \times 10^{-17}(971/(1-w))$	UMIST
$k_{cp,4}$	$HDO + CRPhot \rightarrow OD + H$	$0.75 \times 1.3 \times 10^{-17}(971/(1-w))$	UMIST
$k_{cp,5}$	$HDO + CRPhot \rightarrow OH + D$	$0.25 \times 1.3 \times 10^{-17}(971/(1-w))$	UMIST

Ref. UMIST: Woodall et al. (2007).

Only reactions (4) ($OH + H \rightarrow O + H_2$) and (17) ($OD + H \rightarrow OH + D$) have very different rates, reaction (17) being much faster. However, those reactions are important at low A_V only where photodissociation dominates as destruction process. We assume that $k_6 \simeq k_{24}$.

The hydroxyl radical deuterium fractionation reads

$$f(\mathrm{OD}) = \frac{[\mathrm{OD}]/[\mathrm{OH}]}{[\mathrm{HD}]/[\mathrm{H_2}]} = \frac{D_{\mathrm{OH}}}{D_{\mathrm{OD}}} \left(\frac{k_{16}([\mathrm{OH}]/[\mathrm{O}])[\mathrm{D}] + k_{12}[\mathrm{HD}] + (J_{7b} + k_{23}[\mathrm{H}] + k_{\mathrm{cp},4})X_{\mathrm{D}}([\mathrm{H_2O}]/[\mathrm{O}])}{k_1[\mathrm{H_2}] + (J_6 + k_8[\mathrm{H}] + k_{\mathrm{cp},3})([\mathrm{H_2O}]/[\mathrm{O}])} \right) \Big/ \left(\frac{[\mathrm{HD}]}{[\mathrm{H_2}]} \right). \quad (23)$$

The OD fractionation increases with larger amount of OH and atomic deuterium, and decreases if oxygen is in the atomic form and deuterium is locked in HD. Large amount of OH allows the deuterium exchange reaction to occur.

The knowledge of the abundances of H, H_2, D and HD is needed to estimate the hydroxyl deuterium fraction $f(\mathrm{OD})$.

2.3 H and H_2

The formation of H_2 occurs mostly on grain surface when the grain temperature is below 1000 K and the destruction is caused by photodissociation at low A_V and cosmic ray/X-ray induced ionization and reaction with He^+ in the UV free region. The temperature is low enough to avoid H_2 destruction by atomic hydrogen. The steady-state balance between formation and destruction is

$$R_1(T_g, T_d) n_H[H] = (f_{ss} J_1 + k_{\zeta,4} + k_{35}[He^+])[H_2], \quad (24)$$

where f_{ss} is the H_2 self-shielding function (Draine & Bertoldi 1996) and $R_1(T_g, T_d)$ the molecular hydrogen formation rate on grain surfaces (Tielens 2005):

$$R_1(T_g, T_d) = 4.4 \times 10^{-17} S(T_g, T_d) \left(\frac{T_g}{100} \right)^{1/2}, \quad (25)$$

where T_g and T_d are the gas and dust grain temperature, respectively, and the sticking coefficient S is defined as

$$S(T_g, T_d) = \frac{1}{1 + 4 \times 10^{-2}(T_g + T_d)^{1/2} + 2 \times 10^{-3} T_g + 8 \times 10^{-6} T_g^2}. \quad (26)$$

The sticking coefficient ensures that at high dust temperature atomic hydrogen does not stick on to grain surfaces. The number density of nuclei is

$$n_H = [H] + 2[H_2]. \quad (27)$$

We obtain the atomic and molecular abundances:

$$[H] = n_H \left(\frac{f_{ss} J_1 + k_{\zeta,4} + k_{35}[He^+]}{2R_1 n_H + f_{ss} J_1 + k_{\zeta,4} + k_{35}[He^+]} \right) \simeq n_H \left(\frac{f_{ss} J_1 + k_{\zeta,4}}{2R_1 n_H + f_{ss} J_1 + k_{\zeta,4}} \right) \quad (28)$$

and

$$[H_2] = n_H \left(\frac{R_1 n_H}{2R_1 n_H + f_{ss} J_1 + k_{\zeta,4} + k_{35}[He^+]} \right) \simeq n_H \left(\frac{R_1 n_H}{2R_1 n_H + f_{ss} J_1 + k_{\zeta,4}} \right). \quad (29)$$

Atomic and molecular hydrogen abundances are determined by the gas temperature, density, UV flux, extinction, the self-shielding function and cosmic ray flux.

2.4 D and HD

While H_2 is predominately formed on grain surfaces, formation of HD can also occur in the gas phase by reaction between D and H_2 at high temperature and at density higher than about $5 \times 10^3\,cm^{-3}$ (Le Petit, Roueff & Le Bourlot 2002). HD is destroyed by photodissociation and reaction with atomic H while H_2 is mainly photodissociated. H_2 can self-shield against photodissociation, HD is shielded by dust only. Therefore, deuterium remains atomic at higher extinction than H_2. In hot and dense regions, an important formation route of HD is therefore: $H_2 + D \rightarrow HD + H$ (reaction 10 with a barrier $E_a = 3820\,K$). Larger amount of atomic deuterium is needed to obtain high OD over OH ratio. The production of atomic deuterium is enhanced at high temperature via the conversion reaction $HD + H \rightarrow H_2 + D$. Another destruction mechanism of HD molecules involves photodissociation: $HD + h\nu \rightarrow H + D$. Finally, reaction with H exchanges the atomic hydrogen with atomic deuterium: $HD + H \rightarrow H_2 + D$. At high A_V, cosmic rays destroy HD. Reactions with H^+ and atomic oxygen also destroy HD. The steady-state balance for [HD] then reads

$$[HD] = \frac{(k_{10}[H_2] + R_2 n_H)[D] + k_{37}[D^+][H_2]}{J_2 + k_{\zeta,5} + k_{\zeta,6} + k_{11}[H] + k_{36}[H^+] + (k_{12} + k_{14})[O] + k_{18}[OH]}, \quad (30)$$

where R_2 is the formation rate on grain surfaces (Le Petit et al. 2002) density,

$$R_2(T_g, T_d) = 6.3 \times 10^{-17} S(T_g, T_d) \left(\frac{T_g}{100} \right)^{1/2}, \quad (31)$$

and n_H is the total number. This H_2 formation rate does not take into account grain chemisorption sites contrary to more sophisticated H_2 formation model (Cazaux & Tielens 2002). We assume $k_{\zeta,5} + k_{\zeta,6} \simeq k_{\zeta,4}$ and that the sticking coefficient is the same as for H_2.

We neglect the formation of HD via reaction with D^+ and destruction via reactions with the protons, atomic oxygen and OH radicals. The steady-state balance leads to

$$\frac{[D]}{[HD]} = \frac{J_2 + k_{\zeta,4} + k_{11}[H]}{k_{10}[H_2] + R_2 n_H}. \quad (32)$$

If we can assume that most of the deuterium is locked in H and HD,

$$n_D \simeq [D] + [HD], \quad (33)$$

then we obtain HD and D abundances:

$$[HD] = n_D \left(\frac{k_{10}[H_2] + R_2 n_H}{J_2 + k_{\zeta,4} + k_{11}[H] + k_{10}[H_2] + R_2 n_H} \right) \quad (34)$$

and

$$[D] = n_D \left(\frac{J_2 + k_{\zeta,4} + k_{11}[H]}{J_2 + k_{\zeta,4} + k_{11}[H] + k_{10}[H_2] + R_2 n_H} \right). \quad (35)$$

At low A_V, destruction of [HD] is dominated by photodissociation and at gas temperature a few 100 K, the formation of HD via reaction of atomic deuterium with molecular hydrogen is negligible,

$$\frac{[D]}{[HD]} \simeq \frac{J_2}{R_2 n_H}. \quad (36)$$

Even in obscured ($J_2 \sim 0$) and fully molecular regions ($[H] \sim 0$), cosmic rays induced photodissociation and deuterium exchange reactions ensure that some atomic deuterium always remains in atomic form:

$$\frac{[D]}{[HD]} \simeq \frac{k_{\zeta,4}}{R_2 n_H}. \quad (37)$$

The formation of HD on grains decreases dramatically for dust grain temperature above 100 K.

2.5 Neutral and ionized helium

Where the steady-state abundance of ionized helium is given by the expression

$$[\mathrm{He}^+] = \frac{k_{\zeta,3}[\mathrm{He}]}{k_{35}[\mathrm{H_2}] + k_{\mathrm{e}^-,3}[\mathrm{e}^-]}. \tag{38}$$

Combining with the element conservation equation

$$n_{\mathrm{He}} = [\mathrm{He}] + [\mathrm{He}^+], \tag{39}$$

we obtain

$$[\mathrm{He}^+] = \frac{k_{\zeta,3} n_{\mathrm{He}}}{k_{35}[\mathrm{H_2}] + k_{\mathrm{e}^-,3}[\mathrm{e}^-] - \mathrm{k}_{\zeta,3}}. \tag{40}$$

The He$^+$ abundance can be estimated only if the electron abundance is known. Our simple analytical analysis cannot provide an estimate of the He$^+$ abundance and we will omit in the rest of the paper reactions with He$^+$.

2.6 Water fractionation ratio *f*(HDO)

The results of the previous sections can be combined to derive an analytical formula of the [HDO]/[H$_2$O] ratio:

$$X_{\mathrm{D}} = \frac{[\mathrm{HDO}]}{[\mathrm{H_2O}]} = \mathrm{num/den}, \tag{41}$$

where

$$\mathrm{num} = \frac{k_{22}}{k_5}\left(\frac{D_{\mathrm{OH}}}{D_{\mathrm{OD}}}\frac{D_{\mathrm{H_2O}}}{D_{\mathrm{HDO}}}\right)\frac{k_{16}([\mathrm{OH}]/[\mathrm{O}])[\mathrm{D}] + k_{12}[\mathrm{HD}]}{k_1[\mathrm{H_2}] + (J_6 + k_8[\mathrm{H}] + k_{\mathrm{cp},3})([\mathrm{H_2O}]/[\mathrm{O}])} + \frac{k_{20}}{k_5}\frac{[\mathrm{HD}]}{[\mathrm{H_2}]} \tag{42}$$

and

$$\mathrm{den} = 1 - \frac{k_{22}}{k_5}\left(\frac{D_{\mathrm{OH}}}{D_{\mathrm{OD}}}\frac{D_{\mathrm{H_2O}}}{D_{\mathrm{HDO}}}\right)\frac{(J_{7b} + k_{23}[\mathrm{H}] + k_{\mathrm{cp},4})([\mathrm{H_2O}]/[\mathrm{O}])}{k_1[\mathrm{H_2}] + (J_6 + k_8[\mathrm{H}] + k_{\mathrm{cp},3})([\mathrm{H_2O}]/[\mathrm{O}])}. \tag{43}$$

The abundances and abundance ratios in num and den have been derived earlier:

$$\frac{[\mathrm{OH}]}{[\mathrm{O}]} \simeq \frac{k_1[\mathrm{H_2}]}{J_4 + k_4[\mathrm{H}] + k_{28}[\mathrm{CO}] + k_{29}[\mathrm{C}] + k_{39}[\mathrm{C}^+] + k_{44}[\mathrm{He}^+] + k_{\mathrm{cp},1}}, \tag{44}$$

$$\frac{[\mathrm{H_2O}]}{[\mathrm{OH}]} = \frac{k_5[\mathrm{H_2}]}{J_6 + k_8[\mathrm{H}] + k_{41}[\mathrm{He}^+] + k_{\mathrm{cp},3}}, \tag{45}$$

and combining the two equations above, we obtain

$$\frac{[\mathrm{H_2O}]}{[\mathrm{O}]} = \frac{k_1 k_5[\mathrm{H_2}]^2}{(J_4 + k_4[\mathrm{H}] + k_{28}[\mathrm{CO}] + k_{29}[\mathrm{C}] + k_{39}[\mathrm{C}^+] + k_{44}[\mathrm{He}^+] + k_{\mathrm{cp},1})(J_6 + k_8[\mathrm{H}] + k_{41}[\mathrm{He}^+] + k_{\mathrm{cp},3})}. \tag{46}$$

The water fractionation is composed of three terms. At gas temperature greater than 200 K, the second term k_{12}/k_1 dominates for both low and high extinction and the fractionation reaches 10–1000. Our analysis concerns high-temperature gas only. In warm and dense region, the main oxygen carrier is water and that of carbon is methane CH$_4$ and not CO at high A_{V} and C$^+$ at low A_{V}. As stated before, we further neglect reactions with He$^+$.

At temperature below 100 K, the only fast chemical reactions are between ions and neutral species, which are not taken into account in our analysis. The starting point of water formation is $\mathrm{H_3^+}$. Deuterium enrichment occurs via the deuterated equivalent of $\mathrm{H_3^+}$ and $\mathrm{H_2D^+}$. $\mathrm{H_2D^+}$ has a lower zero-point energy, which favours the deuteration reaction $\mathrm{H_3^+ + HD \rightarrow H_2D^+ + H_2}$. The rate of the back reaction has an energy barrier of 230 K.

The water deuteration fraction enhancement is caused by the fast deuterium exchange reaction with OH (D+OH $\rightarrow$ OD + H). The inverse reaction has an energy barrier of 717 K. Significant amount of atomic deuterium is possible at low and intermediate extinction. We plotted in Fig. 1, the ratio [HDO]/[H$_2$O] as function of the gas temperature for an impinging UV enhanced by a factor of 10^4 and 10^2, for different extinctions ($A_{\mathrm{V}} = 1, 5, 10, 15$), and for two gas densities ($n_{\mathrm{H}} = 10^8$ and 10^{12} cm^{-3}). Disc surfaces around young accreting T Tauri stars receive $\sim 10^4$ to 10^6 times the amount of standard interstellar UV. The UV field, extinction, density and gas temperature values are typically found in regions of discs where water is abundant. In the following section, we will use a time-dependent thermo-photochemical code to support our assumed values for the parameters. The figure shows that large f(HDO) = [HDO]/[H$_2$O] ratios (up to a few hundreds) are possible for gas temperatures up to 500–600 K and up to extinction of 10, although the average value for f is lower than 10. At $T > 500$, the back reaction OD+H $\rightarrow$ OH+D starts to destroy efficiently OD. The figure also shows the large range of values for f(HDO) (0.1–10^3). The f(HDO) curves testify of the sensitivity of the abundances on the gas temperature, which reflects the exponential nature of the Arrhenius' law for neutral–neutral reactions.

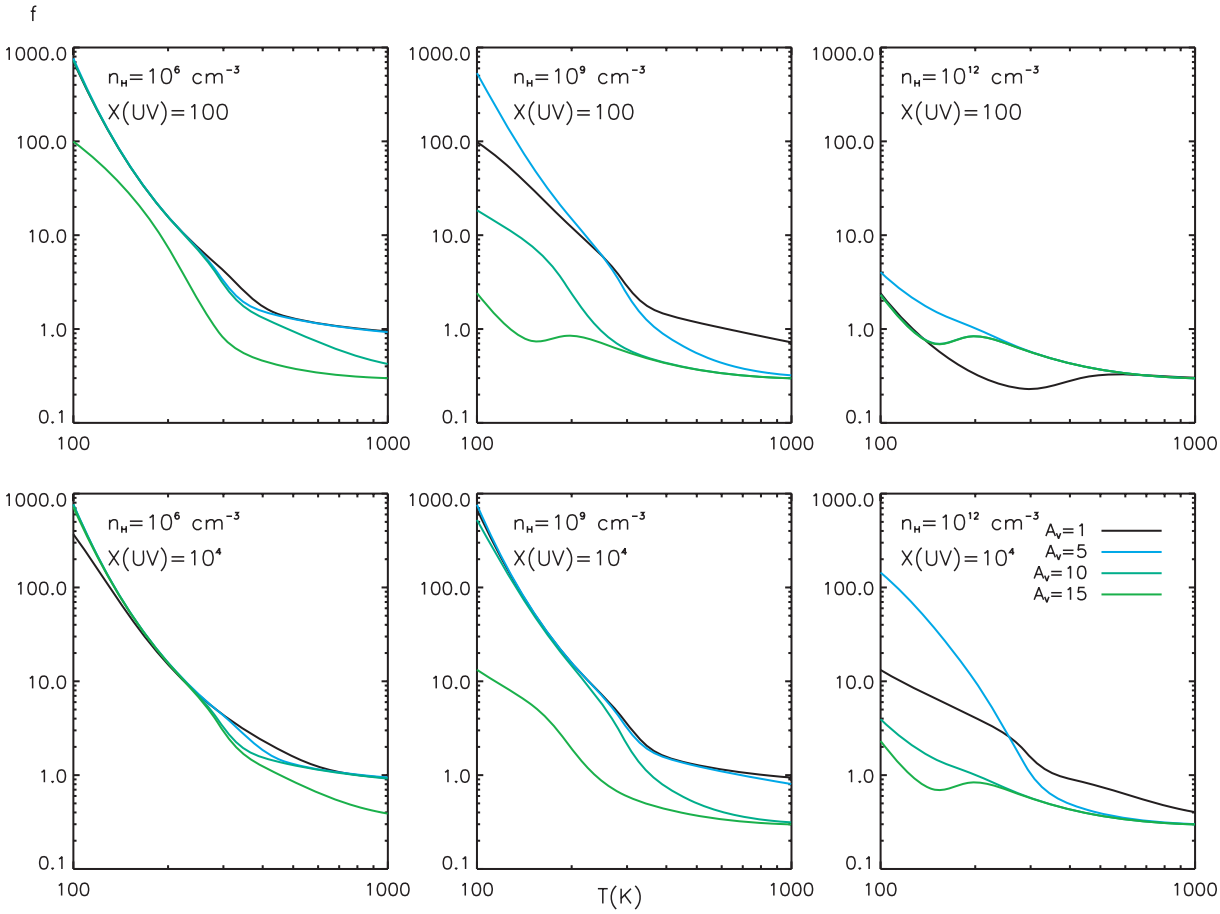

Figure 1. Water deuteration fraction f(HDO). The upper panels show models with UV enhancement of factor 100 with respect to the standard interstellar UV field and for three increasing gas densities. The four curves correspond to the various dust extinctions. The lower panels are models with UV enhancement of 10^4. (See the online version of this article for the colour figure.)

3 TIME-DEPENDENT MODELLING

3.1 ProDiMo photochemical code

We modelled the chemical abundances of a $10^{-3}\,M_\odot$ disc around a typical T Tauri star ($T_{\rm eff}$ 4400 K, $\log g = 4.0, Z = 1.0$) using the photochemical code ProDiMo. ProDiMo combines frequency-dependent 2D dust-continuum radiative transfer, kinetic gas-phase and UV photochemistry, ice formation and detailed non-LTE heating and cooling balance. The major improvement over previous studies is that the density structure is determined by the gas pressure that is computed by detailed chemistry and energy balanced and not by assuming that the gas and dust have the same temperature. Detailed description of the code are given by Woitke, Kamp & Thi (2009a) and in Kamp et al. (2009). The code has been used to determine the water abundance in the inner disc around a typical Herbig Ae star (Woitke et al. 2009b). The most recent additions to the code includes polycyclic aromatic hydrocarbon (PAH) chemistry, time-dependent chemistry, deuterium chemistry and generation of spectral energy distribution and spectral lines. The last two features are not used in the modelling performed for this paper. Table 6 summarized the input parameters to the model. The stellar spectrum was generated using PHOENIX (Brott & Hauschildt 2005) with the addition of chromospheric flux from HD 129333 (Dorren & Guinan 1994). Although the model extends to 300 au, we focus here only on the inner 3 au as we are interested in the [HDO]/[H_2O] ratio in the terrestrial planet forming region of discs.

The chemical network includes a total of 187 deuterated and non-deuterated gas and ice species. Most reaction rates are taken from the UMIST data base (Woodall et al. 2007). Additional reaction rates were compiled from the National Institute of Standards and Technology (NIST) chemical kinetic data base. The rates involving deuterated species are described in e.g. Roberts, Herbst & Millar (2004), Roberts & Millar (2000), Charnley, Tielens & Rodgers (1997) and Brown & Millar (1989). Species can freeze out on to grain surfaces and desorb thermally or upon absorption of a cosmic ray or a UV photon (photodesorption). Grain surface reactions were omitted apart from the grain surface formation of H_2 and HD (Cazaux & Tielens 2002). The photodissociation cross-sections are taken from the Leiden data base described in van Dishoeck, Jonkheid & van Hemert (2008).

The chemical abundances in the disc were established in three stages. First, ProDiMo determined the UV field, hydrostatic density, gas and dust temperature and chemical abundance structure self-consistently assuming steady-state chemistry. Secondly, we computed the

Table 6. Stellar and disc parameters.

Stellar mass	M_*	$0.8\,M_\odot$
Stellar luminosity	L_*	$0.7\,L_\odot$
Effective temperature	$T_{\rm eff}$	4400 K
Disc mass	$M_{\rm d}$	$10^{-3}\,M_\odot$
Disc inner radius	$R_{\rm in}$	0.1 au
Disc outer radius	$R_{\rm out}$	300 au
Vertical column density power law index	ϵ	1
Dust to gas mass ratio		0.01
Dust grain material mass density	$\rho_{\rm dust}$	$2.5\,{\rm g\,cm^{-3}}$
Minimum dust particle size	$a_{\rm min}$	0.01 μm
Maximum dust particle size	$a_{\rm max}$	100 μm
Dust size distribution power law	p	3.5
Cosmic ray flux	CR	$1.7 \times 10^{-17}\,{\rm s^{-1}}$
ISM UV field with respect to Draine field	χ	1.0
Abundance of PAHs relative to ISM	$f_{\rm PAH}$	0.1
α viscosity parameter	α	0.0

Table 7. Typical diffuse cloud abundances used as initial abundances for the molecular cloud chemical calculation. Species with ionization potential (IP) higher than 13.6 eV are neutral while species with IP below 13.6 eV are ionized. The other species have negligible initial abundance.

Species	$\log[n({\rm X})/n_{\rm H}]$
H	0.0
D	−5.0
He	−1.125
C^+	−3.886
O	−3.538
N	−4.67
S^+	−5.721
Si^+	−5.1
Mg^+	−5.377
Fe^+	−5.367
PAH	−6.52

chemical abundances of gas and solid species for a 1-Myr-old molecular cloud with density of $5 \times 10^4\,{\rm cm^{-3}}$ and gas and dust temperature of 15 K from diffuse cloud initial abundances, where the elements are in neutral or ionized atomic form (see Table 7). Thirdly, we ran ProDiMo in the time-dependent chemical mode to simulate the chemical structure of a 1-Myr-old disc using the results of the molecular cloud run as initial chemical abundances and the disc properties computed in the first stage. All other disc properties (UV field, density and temperature structure) were fixed in this last stage.

The three-stage method mimics the incorporation of molecular cloud materials and their subsequent evolution in the disc. It also makes it possible to compare the chemical abundances obtained with the time-dependent model and at steady state. Our approach differs from Visser et al. (2009) who solve the chemistry in a Lagrangian frame and their disc evolves according to viscous spreading. However, their number of species and reactions are limited.

3.2 Model results

Fig. 2 shows the UV field, density and gas and dust temperature structure in the inner 3 au. The disc structure is discussed in Woitke et al. (2009a). In this paper, we focus on the water and HDO abundances. Fig. 3 shows the water and HDO abundances at steady state on the left and for a disc of 1 Myr old on the right. Apart from the water and HDO in the mid-plane beyond ∼1.5–2 au , the water and HDO abundances are similar for the steady-state and time-dependent chemistry models. The differences stem from the fact that at steady state even very slow reactions will impact the chemistry. In this case, the dust temperature is low enough ($T_{\rm d} < 150\,{\rm K}$) such that all water and HDO should be frozen out. In the time-dependent model, significant amount of water and HDO remains in the gas phase in the inner 1 au or above the ice zone. The differences between the steady-state and time-dependent abundances occur in low gas-phase water abundance regions and thus do not impede our analysis of deuterium enrichment for gas-phase water either outside the water freeze-out zone.

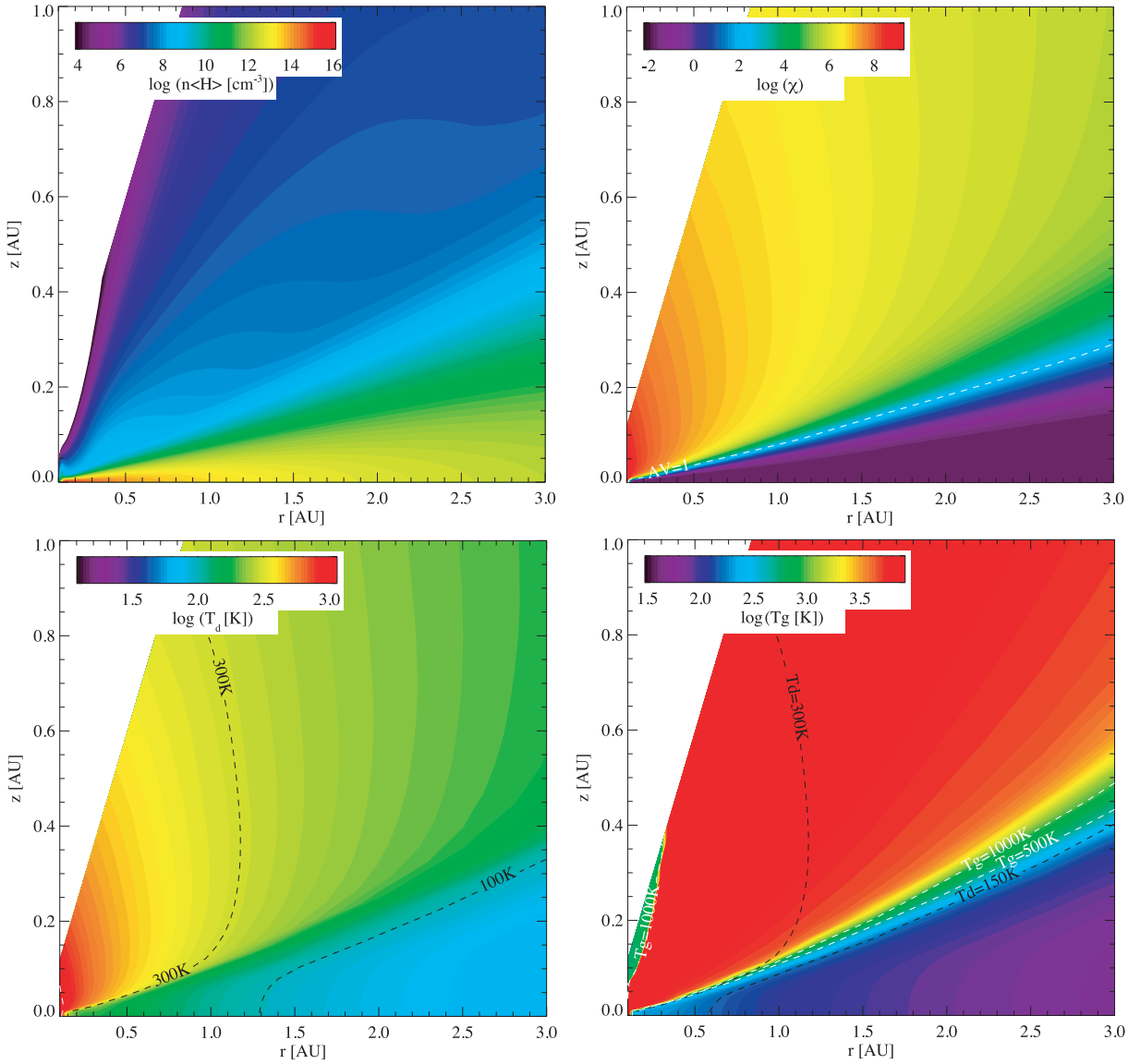

Figure 2. The four panels show the gas density $n_{<\mathrm{H}>}$ (upper left), strength of the UV field with respect to the Draine field χ (upper right), the dust temperature T_d (lower left) and the gas temperature T_g with dust and gas temperature overlaid (lower right) for the inner 3 au computed by ProDiMo. The structure is consistent with the chemical abundances. (See the online version of this article for the colour figure.)

The [HDO]/[H_2O] ratio for the time-dependent model is plotted in Fig. 4. The water abundance levels at 10^{-6} and 10^{-8} are overlaid. Water is abundant as soon as hydrogen is in molecular form. In our model, water and HDO are frozen on to grain surfaces in the mid-plane beyond ∼1.5 au as shown in Fig. 5. The gas-phase [HDO]/[H_2O] ratio decreases with radius. At 0.5–1.5 au in the mid-plane, the ratio is a few 10^{-3}–10^{-2}. Gas-phase water and HDO are located in three zones: the inner mid-plane, the cold belt and the hot layer (Woitke et al. 2009b). The mass and average gas and dust temperature are given in Table 8.

Most of the gas-phase water [$n(H_2O)/n_\mathrm{H} = 10^{-8}$–$10^{-5}$] is located in the inner plane close to the star ($R < 1$ au). In the inner 30 au, a small fraction is found above the mid-plane (Woitke et al. 2009b), where the vertical extinction A_V is between 1 and 10. Although of insignificant mass, the molecules are hot and emit strongly (e.g. Carr & Najita 2008; Salyk et al. 2008). In the outer disc, gas-phase water is found in a cold belt, which is sandwiched between $A_\mathrm{V} \sim 1$ and 5 where efficient photodesorption maintains some water molecules in the gas phase (see Woitke et al. 2009b). Since HDO and H_2O have similar adsorption energy, the gas-phase abundance of both species are co-located (see Fig. 3). We plotted the vertical column densities for H, D, OH, OD, H_2O, HDO, H_2O# and HDO# in Fig. 6. This figure shows that the column density ratios HDO/H_2O, HDO#/H_2O# and OD/OH stay relatively constant in the inner disc, with values much higher than the elemental D/H ratio of 10^{-5}.

In the high water abundance region, the [HDO]/[H_2O] ratio is higher than 10^{-2}. Using the mass of H_2O and HDO in the inner mid-plane listed in Table 8, we derived an average [HDO]/[H_2O] ratio of 4.6×10^{-3}, which is 30 times higher than the Earth Mean Ocean Water value ($\simeq 1.49 \times 10^{-4}$) and close to cometary values. The actual [HDO]/[H_2O] values in our models depend on the disc parameters. Future studies will focus on the effect of disc properties (disc mass, radius, ...) on the [HDO]/[H_2O] ratios.

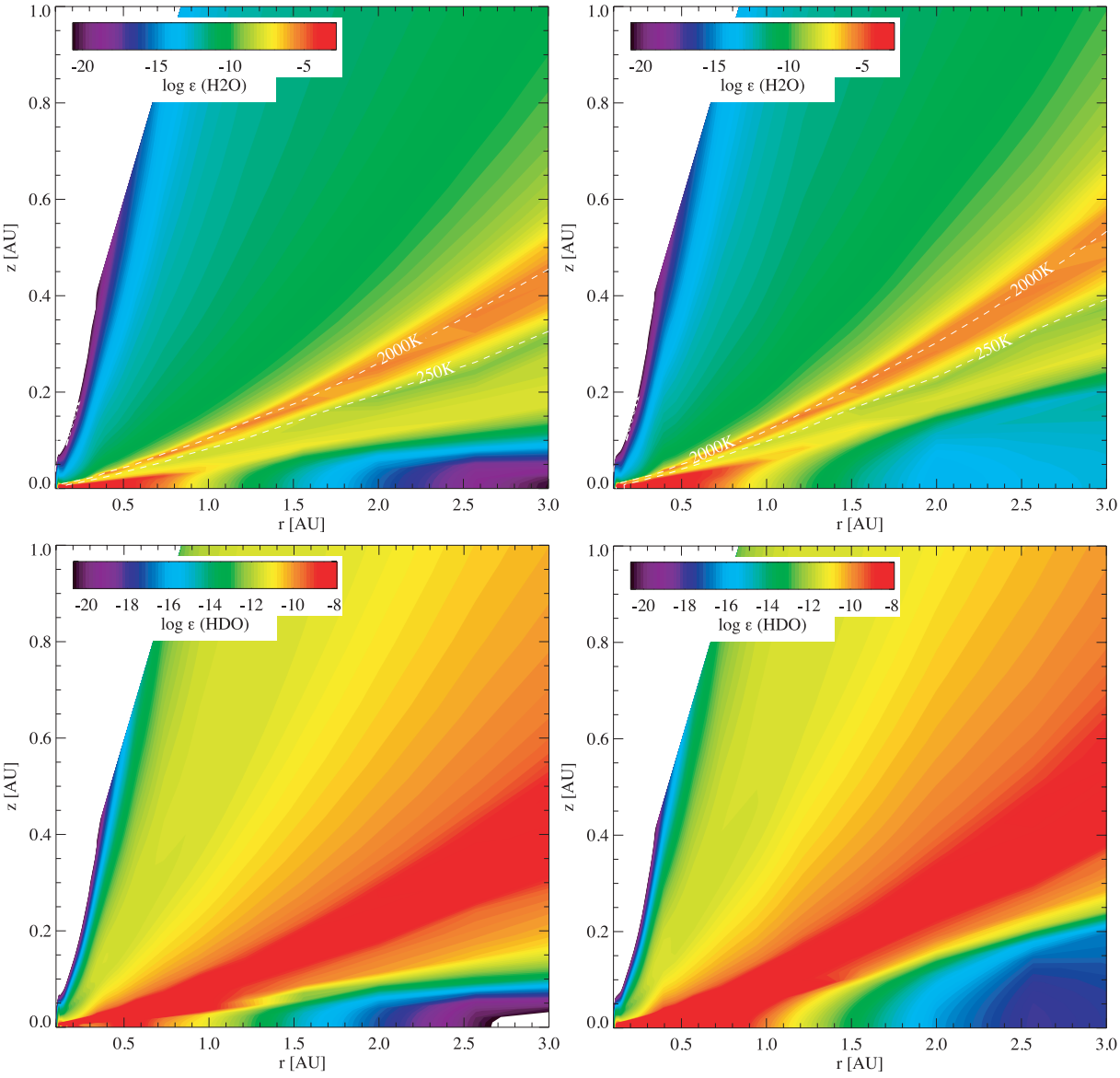

Figure 3. Gas-phase H_2O and HDO abundance in the inner 3 au computed by ProDiMo. The left-hand panels show the steady-state abundances while the right-hand panels show the time-dependent abundances for a 1-Myr-old disc. (See the online version of this article for the colour figure.)

Overall, the [HDO]/[H_2O] ratios in the inner disc mid-plane by the time-dependent code ProDiMo are consistent with the analytical results. Our results contradict the simple decrease in [H_2O]/[HDO] with increasing temperature if thermochemical equilibrium ratios are assumed.

4 DISCUSSION AND CONCLUSION

A simple analytical analysis shows that high water fraction is possible in a simple deuteration chemical network for gas hotter than 100 K if neutral–neutral reactions are included. The analytical results are supported by the time-dependent photochemical model results. In their study, Willacy & Woods (2009) also found that HDO can be abundant in the inner disc.

The water deuterium fractionation is determined by the ratio between the rate of formation of OD via O + HD and the rate of formation of OH via O + H_2. Lower zero-point energy for HD makes the first reaction faster than the second one above 200 K. At low temperature ($T < 100$ K), fast deuteration of H_3^+, the main driver of cold gas-phase chemistry ensures that main molecules are deuterium-enriched. Another reason for higher HDO/H_2O is the preferential branching into OD + H when HDO is photodissociated (Shafer et al. 1989; Vander Wal et al. 1990, 1991).

From our work, it is also theoretically possible to have high water deuterium fractionation from gas-phase photochemistry above 200 K. Deuterium enrichment can also occur at high temperature because of the energy difference in activation barrier for deuterium exchange and the back reactions. Finally, water deuterium enrichment is not as stringent a constraint as thought for the origin of water on the Earth.

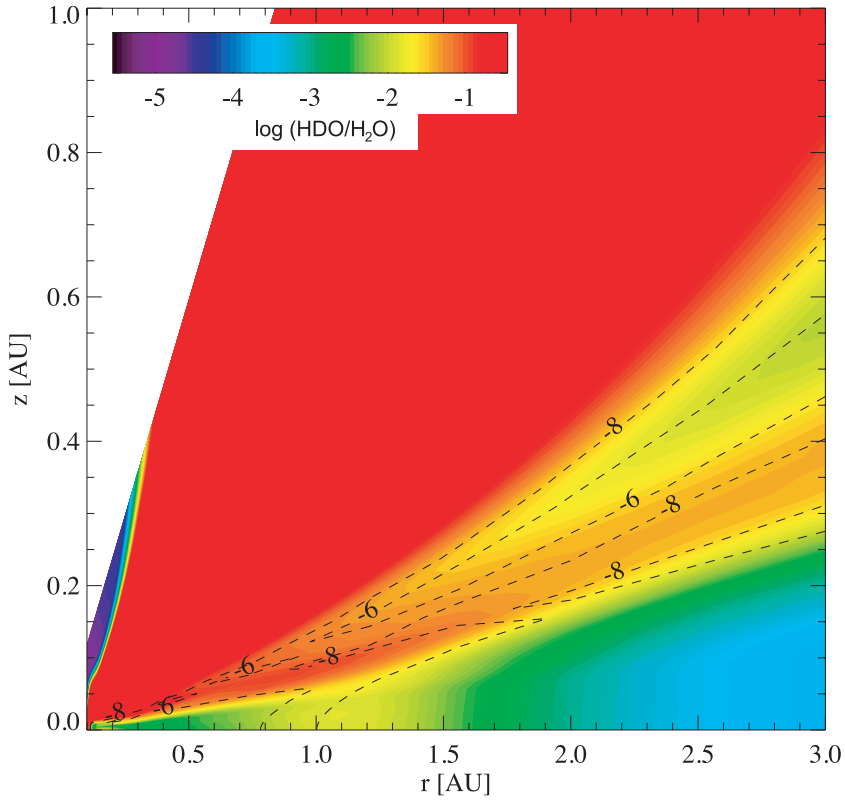

Figure 4. [HDO]/[H_2O] in the 3 au of a 10^{-3} disc as computed by the photochemical code ProDiMo. The contours indicate the regions where gas-phase water abundance is 10^{-6} and 10^{-8}.

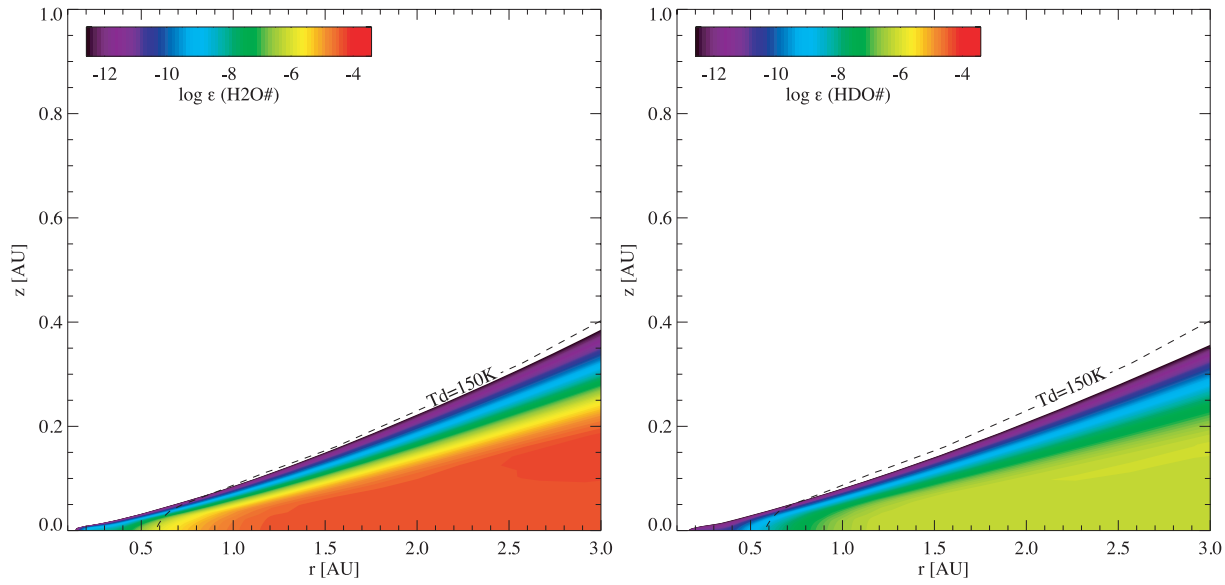

Figure 5. H_2O and HDO ice abundance in the inner 3 au. The dash line indicate the region where the dust temperature is 150 K. H_2O and HDO freeze at ∼150 K. (See the online version of this article for the colour figure.)

Deuterium-enriched water may have been synthesized at ∼1 au and incorporated directly on to silicate dust grains (Stimpfl et al. 2006). Water could have been incorporated on the Earth already at the stage of planetesimals accretion. However, our simple analytical steady-state chemical model and the 2D modelling with ProDiMo do not include effects of turbulent mixing in protoplanetary discs, both radial and vertical.

Table 8. Mass and average gas and dust temperature for the three gas-phase water and HDO locations. The paper focuses mostly on the inner mid-plane.

Location	Mass ($M_\odot$)	$\langle T_{gas} \rangle$ (K)	$\langle T_{dust} \rangle$ (K)
		H_2O	
Inner mid-plane	2.6×10^{-8}	178	177
Cold belt	1.1×10^{-9}	16	16
Hot layer	2.1×10^{-12}	1147	120
		HDO	
Inner mid-plane	1.2×10^{-10}	140	140
Cold belt	3.8×10^{-11}	16	16
Hot layer	2.6×10^{-14}	474	102

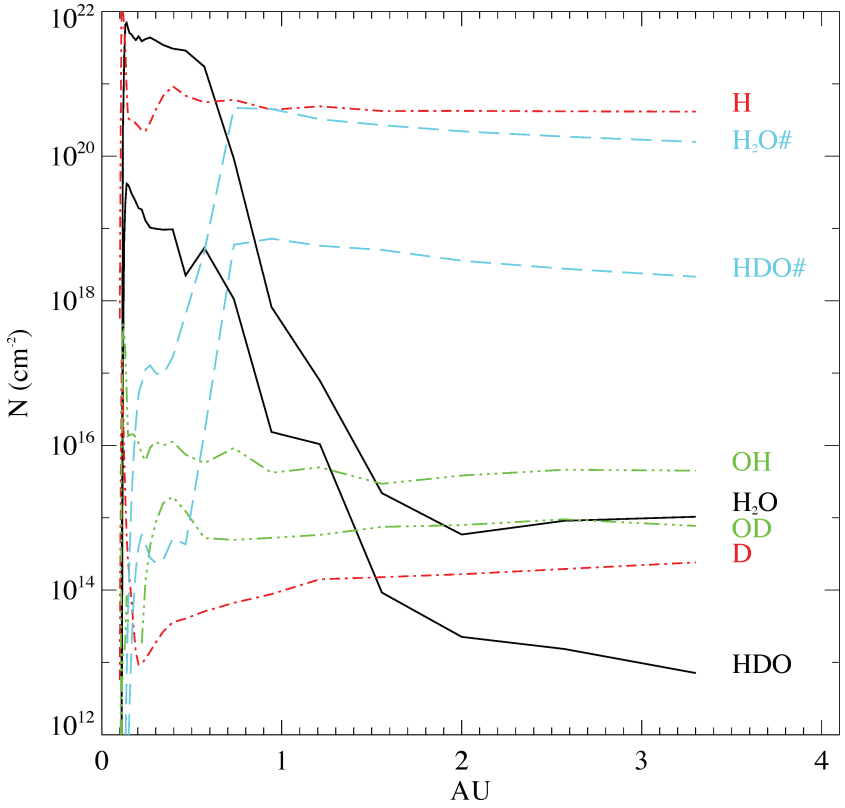

Figure 6. Half disc vertical column density for various species in the inner 3 au. (See the online version of this article for the colour figure.)

ACKNOWLEDGMENTS

W-FT is supported by a Scottish Universities Physics Alliance (SUPA) fellowship in Astrobiology. We thank the referee for his/her comments.

REFERENCES

Bergin E. A., Neufeld D. A., Melnick G. J., 1998, ApJ, 499, 777
Brott I., Hauschildt P. H., 2005, in Turon C., O'Flaherty K. S., Perryman M. A. C., eds, The Three-Dimensional Universe with Gaia, ESA SP-576. ESA, Noordwijk p. 565
Brown P. D., Millar T. J., 1989, MNRAS, 237, 661
Carr J. S., Najita J. R., 2008, Sci, 319, 1504
Cazaux S., Tielens A. G. G. M., 2002, ApJ, 575, L29
Ceccarelli C., Dominik C., Caux E., Lefloch B., Caselli P., 2005, ApJ, 631, L81
Charnley S. B., Tielens A. G. G. M., Rodgers S. D., 1997, ApJ, 482, L203
Croswell K., Dalgarno A., 1985, ApJ, 289, 618
Dartois E., Thi W.-F., Geballe T. R., Deboffle D., d'Hendecourt L., van Dishoeck E., 2003, A&A, 399, 1009

Dorren J. D., Guinan E. F., 1994, ApJ, 428, 805
Draine B. T., Bertoldi F., 1996, ApJ, 468, 269
Drake M. J., 2005, Meteoritics Planet. Sci., 40, 519
Genda H., Ikoma M., 2008, Icarus, 194, 42
Gensheimer P. D., Mauersberger R., Wilson T. L., 1996, A&A, 314, 281
Glassgold A. E., Meijerink R., Najita J. R., 2009, ApJ, 701, 142
Gomes R., Levison H. F., Tsiganis K., Morbidelli A., 2005, Nat, 435, 466
Guilloteau S., Piétu V., Dutrey A., Guélin M., 2006, A&A, 448, L5
Hopkins M., Harrison T. M., Manning C. E., 2008, Nat, 456, 493
Kamp I., Tilling I., Woitke P., Thi W., Hogerheijde M., 2009, A&A, 510, 18
Le Petit F., Roueff E., Le Bourlot J., 2002, A&A, 390, 369
Linsky J. L., 2003, Space Sci. Rev., 106, 49
Lyons J. R., Young E. D., 2005, Nat, 435, 317
Morbidelli A., Chambers J., Lunine J. I., Petit J. M., Robert F., Valsecchi G. B., Cyr K. E., 2000, Meteoritics Planet. Sci., 35, 1309
Nuth J. A., 2008, Earth Moon Planets, 102, 435
Parise B., Simon T., Caux E., Dartois E., Ceccarelli C., Rayner J., Tielens A. G. G. M., 2003, A&A, 410, 897
Parise B. et al., 2005, A&A, 431, 547
Prasad S. S., Huntress W. T., Jr, 1980, ApJS, 43, 1
Raymond S. N., Quinn T., Lunine J. I., 2004, Icarus, 168, 1
Raymond S. N., Quinn T., Lunine J. I., 2005, ApJ, 632, 670
Richet P., Bottinga Y., Janoy M., 1977, Annu. Rev. Earth Planet. Sci., 5, 65
Righter K., Drake M. J., Scott E. R. D., 2006, in Lauretta D. S., McSween H. Y., Jr, eds, Meteorites and the Early Solar System II. Univ. Arizona Press, Tucson, p. 803
Robert F., Gautier D., Dubrulle B., 2000, Space Sci. Rev., 92, 201
Roberts H., Millar T. J., 2000, A&A, 361, 388
Roberts H., Herbst E., Millar T. J., 2004, A&A, 424, 905
Salyk C., Pontoppidan K. M., Blake G. A., Lahuis F., van Dishoeck E. F., Evans N. J., II, 2008, ApJ, 676, L49
Shafer N., Satyapal S., Bersohn R., 1989, J. Chem. Phys., 90, 6807
Stimpfl M., Walker A. M., Drake M. J., de Leeuw N. H., Deymier P., 2006, J. Crystal Growth, 294, 83
Talukdar R. K., Gierczak T., Goldfarb L., Rudich Y., Kao B. S. M., Ravishankara A. R., 1996, J. Phys. Chem., 100, 3037
Thi W.-F., Bik A., 2005, A&A, 438, 557
Tielens A. G. G. M., 2005, The Physics and Chemistry of the Interstellar Medium. Cambridge Univ. Press, Cambridge
Vander Wal R. L., Scott J. L., Crim F. F., 1990, J. Chem. Phys., 92, 803
Vander Wal R. L., Scott J. L., Crim F. F., Weide K., Schinke R., 1991, J. Chem. Phys., 94, 3548
van Dishoeck E. F., 1988, in Millar T. J., Williams D. A., eds, Rate Coefficients in Astrochemistry. Kluwer, Dordrecht, p. 49
van Dishoeck E. F., Dalgarno A., 1984, ApJ, 277, 576
van Dishoeck E. F., Jonkheid B., van Hemert M. C., 2008, Faraday Discussion Chem. Soc., 133, 231
Visser R., van Dishoeck E. F., Doty S. D., Dullemond C. P., 2009, A&A, 495, 881
Watson W. D., 1976, Rev. Modern Phys., 48, 513
Willacy K., Woods P. M., 2009, ApJ, 703, 479
Woitke P., Kamp I., Thi W.-F., 2009a, A&A, 501, 383
Woitke P., Thi W.-F., Kamp I., Hogerheijde M. R., 2009b, A&A, 501, L5
Woodall J., Agúndez M., Markwick-Kemper A. J., Millar T. J., 2007, A&A, 466, 1197
Yung Y. L., Wen J.-S., Pinto J. P., Pierce K. K., Allen M., 1988, Icarus, 76, 146
Zhang J. Z., Imre D. G., 1988, Chem. Phys. Lett., 149, 233
Zhang J. Z. H., Miller W. H., 1989, J. Chem. Phys., 91, 1528

This paper has been typeset from a TEX/LATEX file prepared by the author.